ACS APPLIED MATERIALS & INTERFACES

Research Article

www.acsami.org

# Plasmonic Ag@AgCl Nanotubes Fabricated from Copper Nanowires as High-Performance Visible Light Photocatalyst

Lei Sun,[†,‡,∥] Ruizhong Zhang,[†,§,∥] Yuan Wang,[‡] and Wei Chen*[,†]

[†]State Key Laboratory of Electroanalytical Chemistry, Changchun Institute of Applied Chemistry, Chinese Academy of Sciences, Changchun, Jilin 130022, China

[‡]School of Chemistry and Environmental Engineering, Changchun University of Science and Technology, Changchun, Jilin 130022, China

[§]University of the Chinese Academy of Sciences, Beijing 100039, China

Supporting Information

**ABSTRACT:** In this paper, plasmonic photocatalyst Ag@AgCl nanotubes were prepared by a cost-efficient and template-based method and their photocatalytic properties were studied. In the synthesis, copper nanowires were first synthesized and Ag nanotubes were then obtained through the galvanic reaction between copper and Ag ions. The formation of Ag@AgCl nanotubes was finally achieved by in situ oxidation reaction upon the addition of $FeCl_3$. The crystal structure of the product was characterized by X-ray powder diffraction. The morphology and composition of the composite were studied by scanning electron microscopy, transmission electron microscopy, and X-ray photoelectron spectroscopy measurements. All the structure characterizations showed that the tubulate product was produced by the synthetic processes. By using the obtained product as photocatalyst, the photodegradation of methyl orange (MO) was investigated under visible light. The experimental results showed that the as-prepared Ag@AgCl nanotubes exhibit excellent photocatalytic performance and high stability. Under visible light irradiation, more than 92.58% of the MO dye has been decomposed in 10 min on the product with a 1:1 ratio of Fe/Ag. On the basis of the proposed mechanism, the improved photocatalytic activities of the Ag@AgCl hybrids can be ascribed to the enhanced surface area for dye molecule adsorption, enhanced visible light absorbance, and the efficient charge separation of the hybrid nanostructures.

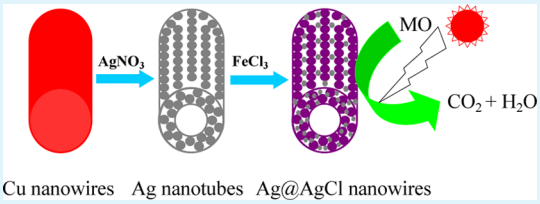


**KEYWORDS:** *photocatalyst, nanotube, plasmon, silver chloride, visible light, dye degradation*

## 1. INTRODUCTION

It is well-known that water is the source of life. However, water pollution has become one of the critical environmental issues around the world. Especially, with the rapid development of industry and modern society, an increasing number of hazardous organic compounds are being discharged into the environment.[1] So far, the semiconductor photocatalytic oxidation method has become more and more popular for solving wasterwater treatment problem.[2,3] Among the photocatalysts, plasmonic photocatalysts based on silver nanoparticles (Ag NPs) and silver halides have attracted much attention in recent years because of their outstanding photocatalytic performance for dye degradation.[4,5] For example, Han et al.[6] prepared a Ag@AgCl cubic photocatalyst via a hydrothermal process. Kuai et al.[7] fabricated a plasmonic Ag/AgBr photocatalyst by hydrothermal and subsequent sunlight-induced reduction processes. Wang et al.[8] synthesized Ag@Ag (Br, I) photocatalyst through a different ion-exchange treatment, followed by a light-induced reduction process. With Ag and AgX (X = Cl, Br, I) as photocatalysts, both the surface plasmon resonance (SPR) absorption of silver nanoparticles and the strong interaction between Ag and AgX contribute to the high photocatalytic activities of the hybrid catalysts. It should be noted that, among the Ag NP-based photocatalysts, their photocatalytic performance is strongly dependent on the size and morphology of the plasmonic materials.[4,9] Recently, Ag@AgCl photocatalysts with various structures, including porous nanocomposites, cube-like, necklace-like, and near-spherical nanocatalysts, have been synthesized and their visible light photocatalysis has been reported.[10−13]

Among the developed functional materials, hollow micro/nanostructures have been extensively investigated due to their novel structure and properties, including highly efficient usage of metals, high surface/interface area, and low refractive index, which are much different from the corresponding bulk materials, and their promising applications in energy storage, sensors, catalysis, etc.[14−16] By far, the template-based method has been widely used to fabricate hollow micro/nanostructures, with which the morphology and dimension of the cavity of the produced hollow structures can be manipulated by the original templates.[15] In recent years, hollow micro/nanostructured photocatalysts have been successfully synthesized and they

Received: February 17, 2014
Accepted: August 15, 2014
Published: August 15, 2014

  

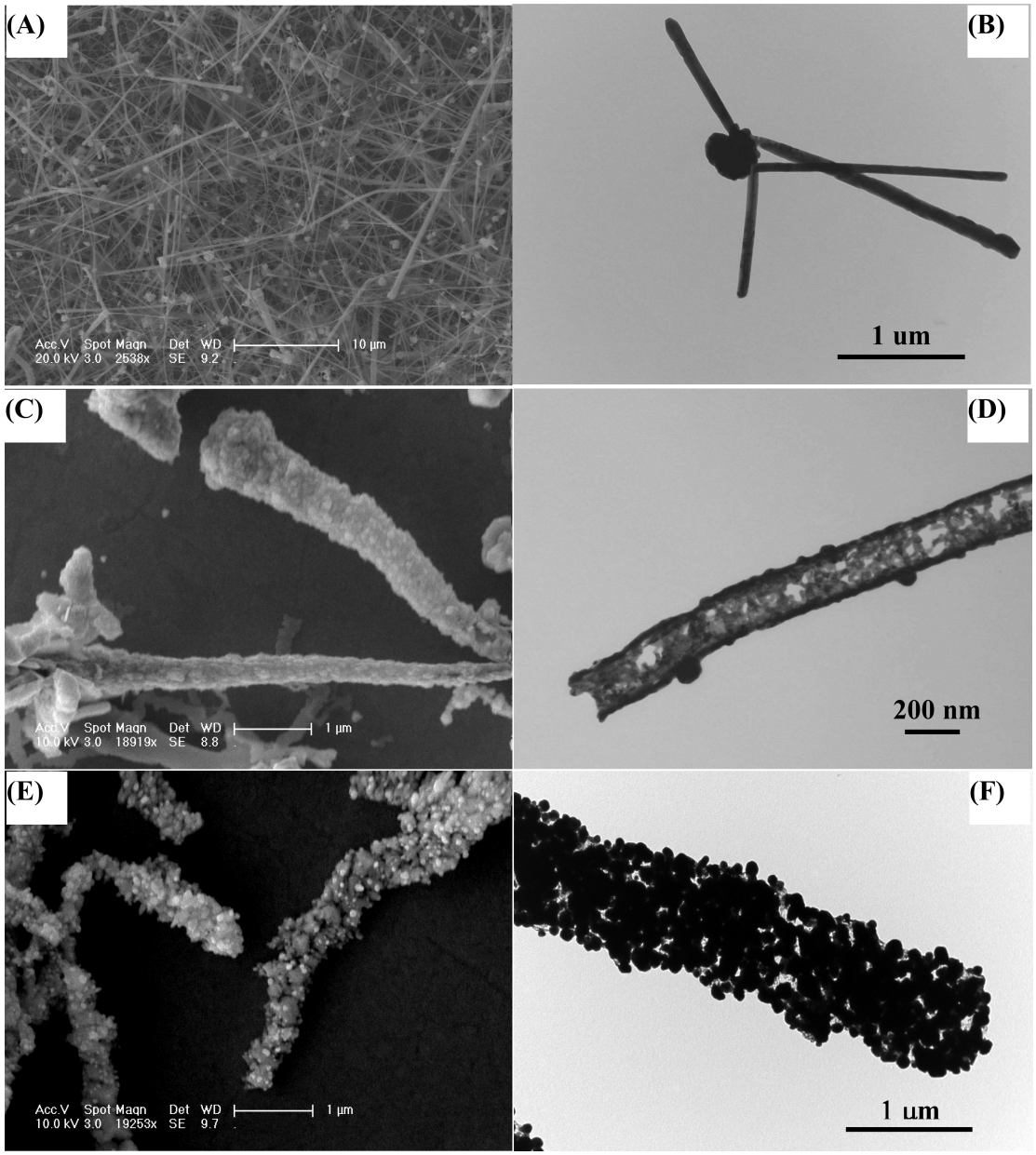


**Figure 1.** SEM (left panels) and TEM (right panels) images of Cu nanowires (A, B), Ag nanotubes prepared via a replacement reaction with the Cu nanowires as sacrificial templates (C, D), and Ag@AgCl nanotubes (E, F).

exhibited excellent photocatalytic activities.[17−20] For instance, by using polymer beads as sacrificial templates,[21] a robust hollow nanostructure composed of $TiO_2$ and graphene nanosheets has been successfully fabricated. The hollow-sphere nanocomposite exhibited excellent photocatalytic performance for the $CO_2$ reduction under UV irradiation. Tang et al.[22] synthesized Ag@AgCl cubic cages and studied their photocatalytic performance for organic dye degradation. In another work, Wang et al.[23] synthesized Ag@AgCl hollow spheres of plasmonic photocatalysts through a chemical reduction route under the visible light irradiation. Among the previous reports, most studies focused on the zero-dimensional plasmonic nanospheres. However, one-dimensional tubulate photocatalysts with a uniform structure have been rarely reported.

Herein, we report a facile process for synthesizing stable and hollow plasmonic photocatalyst Ag@AgCl nanotubes. In the synthesis, Ag nanotubes were first synthesized by using presynthesized Cu nanowires as templates. Ag@AgCl nanotubes were then fabricated from the reaction between Ag nanotubes and $FeCl_3$ at room temperature. The as-synthesized Ag@AgCl nanotubes exhibited high photocatalytic activity and stability for organic dye degradation under visible light irradiation. The excellent photocatalytic activity of the as-prepared Ag@AgCl nanotubes could be mainly ascribed to the unique nanostructure and properties. First, the surface plasmon resonance from the silver component in the hybrid material can effectively improve the efficiency of charge separation. Second, during the process of organic dye degradation, the unique tubulate structures of Ag@AgCl composites can provide inner and outer surfaces for the efficient absorption of dye molecules, resulting in improved photocatalytic efficiency. Finally, the nanotubes can serve as a photon trap-well to allow the multiscattering of incident light and thus result in enhanced light absorption.

## 2. EXPERIMENTAL SECTION

**2.1. Materials.** Copper nitrate trihydrate ($Cu(NO_3)_2{\cdot}3H_2O$), sodium hydroxide (NaOH), ethylenediamine, hydrazine hydrate, silver nitrate ($AgNO_3$), ferric chloride ($FeCl_3$), hydrochloric acid (HCl), methyl orange (MO), Rhodamine B (RhB), polyvinylpyrrolidone (PVP), and ethanol were purchased from Beijing Chemical Works. Phenol was obtained from the Beijing Yili Fine Chemicals Co., Ltd. The commercial P25 $TiO_2$ purchased from Shen Na Trade Co. Ltd. was used for photocatalytic comparison. All chemicals were used without further purification. Ultrapure water (18.3 MΩ cm) was used in all the experiments.

**2.2. Preparation of Cu Nanowires.** Cu nanowires were prepared using a procedure described previously with some minor modifications.[24] In a typical synthesis, 0.3 g of $Cu(NO_3)_2{\cdot}3H_2O$ was dissolved in 10 mL of water and mixed with 200 mL of an aqueous NaOH solution (15 M) in a 500 mL glass bottle. To this, 2 mL of ethylenediamine and 0.5 mL of hydrazine (30%) were added. The flask was then placed in a water bath at 60 °C for 80 min. The produced Cu nanowires were collected by centrifugation, washed thoroughly with water and ethanol to remove ethylenediamine and other impurities, and then dispersed in water for further use.

**2.3. Synthesis of Ag Nanotubes.** In a typical procedure, the as-prepared Cu nanowires were mixed with 100 mL of water in a 500 mL glass bottle. The mixture was sonicated to make the Cu nanowires fully dispersed. Then, 4 g of PVP in 100 mL of water was added to the above solution. Next, 0.5308 g of $AgNO_3$ in 100 mL of water was added dropwise under magnetic stirring at room temperature. The resultant mixture becomes a silk-like gray suspension in a few minutes. The formed Ag nanotubes were centrifuged at 10 000 rpm for 10 min to remove any unreacted starting materials and then dried at 60 °C for 5 h.

**2.4. Synthesis of Ag@AgCl Nanotubes.** In a typical synthesis, a certain amount of $FeCl_3$ (the molar ratios of Ag:Fe = 4:1, 2:1, 4:3, 1:1, and 2:3, respectively) was added drop by drop to the as-prepared silver nanotube (50 mg) solution that contained 30 mg of PVP. Under vigorous stirring at room temperature, the color of the obtained mixture became purple within a certain period of time. The obtained samples were washed with water and ethanol to remove any unreacted starting materials via centrifugation. Finally, the Ag@AgCl nanotubes were dried at 60 °C for 5 h.

**2.5. Characterization.** SEM images were taken with an XL30 field-emission scanning electron microscope at an accelerating voltage of 15 kV. Morphology characterizations were performed with a Hitachi H-600 transmission electron microscope (TEM) with an accelerating voltage of 100 kV. XRD patterns were collected by a D8 ACE (GDVANermany) with Cu-Ka radiation ($\lambda$ = 1.54 Å). XPS analysis was performed on an ESCALAB-MKII X-ray photoelectron spectrometer. UV−vis diffuse reflectance spectra were collected on a Shimadzu UV-3600 spectrophotometer. UV−Vis absorption spectra were obtained from a Shanghai Mapada spectrometer.

**2.6. Photocatalytic Tests.** For a photocatalytic test, 5 mg of the prepared Ag@AgCl photocatalysts was dispersed in 20 mL of 10 mg/L organic molecules (MO, phenol, or RhB) aqueous solution. The mixture was kept in the dark for 60 min to ensure the saturated adsorption of organic dyes on the surface of catalysts. A 500 W Xe arc lamp (CHFXM500W) equipped with a cutoff filter as a visible light source ($\lambda$ > 400 nm) was used to induce the photocatalytic reaction. In a typical measurement, 1 mL of the mixed solution was taken out at different times and centrifuged to separate the Ag@AgCl photocatalysts from solution. The top solution was then added to a quartz cuvette for the absorption spectrum measurements in the range of 200−800 nm.

## 3. RESULTS AND DISCUSSION

**3.1. Materials Characterization.** The morphologies of the synthesized nanomaterials were first characterized by electron microscopy. Figure 1A,B shows the typical SEM and TEM images of the as-obtained Cu nanowires. The average diameter of these Cu nanowires was measured to be 234.8 ± 3.8 nm, and the length of the nanowires could reach about tens of micrometers. It can be seen that nanoparticles are attached on the tips of most Cu nanowires, which is in accordance with the previous report.[25] Such an observation suggests that, in the present synthetic process, copper nanoparticles were first formed as seeds and copper nanowires can then grow from the nanoparticle seeds. Figure 1C,D shows the SEM and TEM images of the product produced through the galvanic reaction between the presynthesized Cu nanowires and $AgNO_3$. Obviously, the morphology of the product is much different from that of the Cu nanowires, and silver nanotubes have been formed via the galvanic reaction. The average diameter of the Ag nanotubes increased to the range of 0.2−1 $\mu$m, and the wall thickness of the nanotubes is between 20 and 40 nm. Note that the inner diameter of the tubes is consistent with that of the Cu nanowires. In the next step, a widely reported in situ oxidation process was used to prepare Ag@AgCl nanotubes by mixing the Ag nanotubes and $FeCl_3$ at room temperature. From the SEM and TEM images shown in Figure 1E,F, tubulate Ag@AgCl were formed and the diameter is further increased to 0.5−1.5 $\mu$m. Interestingly, the nanotubes are composed of nanoparticle assemblies with a rough surface, but they maintain the overall shape of the original silver nanotubes. Such a hollow tubulate structure with porous and rough walls is beneficial for the adsorption and degradation of organic pollutants. To determine the composition of the nanotubes, energy-dispersive X-ray (EDX) was also measured. For the Ag nanotube sample (Figure 2A), there is only a strong signal from Ag and no peak from copper was observed. Such a result indicates that, after the galvanic replacement reaction between Cu nanowires and silver nitrate, the copper nanowire templates have been completely removed and metallic silver nanotubes can be procured. From the EDX spectrum of the Ag@AgCl nanotubes (Figure 2B), both silver and chlorine are present in the sample, suggesting the formation of Ag@AgCl composites. The composition of the nanotubes can also be reflected from the color change. The insets in Figure 2A,B display the color of the Ag and Ag@AgCl nanotubes, respectively. The Ag nanotube sample shows the characteristic silk-like gray color. However, after the oxidation by $FeCl_3$, the suspension exhibit a purple color, suggesting the formation of Ag@AgCl nanotubes.

The crystal structure of the synthesized Ag@AgCl composites was then characterized by XRD. Figure 3 shows the XRD spectra of the copper nanowires, Ag nanotubes, and Ag@AgCl nanotubes. In Figure 3, spectrum A, the XRD pattern of copper nanowires shows three obvious diffraction peaks at $2\theta$ = 44.1, 51.2, and 74.9°, which correspond to the (111), (200), and (220) (JCPDS 65-9092) crystal planes, respectively, of the fcc copper. No diffraction peak from $CuO_x$ and other impurities indicates the high purity of the produced Cu nanowires. In the XRD spectrum of Ag nanotubes, the diffraction peaks at 38.6, 44.7, 64.8, and 77.8° correspond to the planes of (111), (200), (220), and (311) (JCPDS 65-2871) of the Ag fcc structure, respectively. It is worth to note that no characteristic diffraction peaks from the Cu nanowire template can be observed, indicative of the thorough removal of the template and the formation of pure Ag nanotubes. Such a result agrees well with the above EDX analysis (Figure 2A). After the oxidation of Ag nanotubes by $FeCl_3$, the product (Ag@AgCl nanotubes) displays a different XRD pattern (Figure 3C) with distinct diffraction peaks of $2\theta$ at 28.2, 32.6,46.6, 55.2,57.8, 67.8, 74.8, and 77.1°, which can be indexed to the (111), (200),

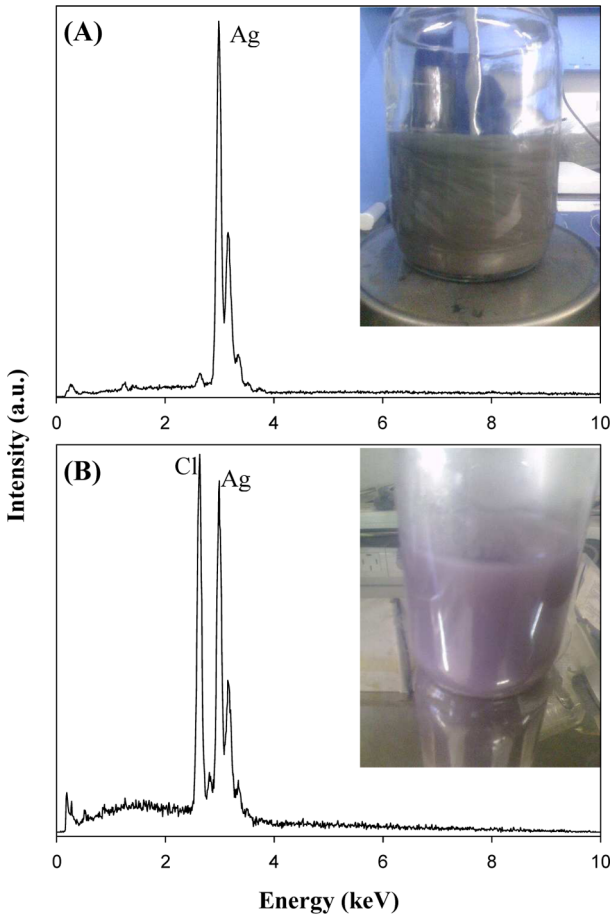


**Figure 2.** EDX spectra of the as-obtained Ag nanotubes (A) and Ag@AgCl nanotubes (B). Insets in A and B show the photographs of the Ag nanotubes and Ag@AgCl nanotubes, respectively.

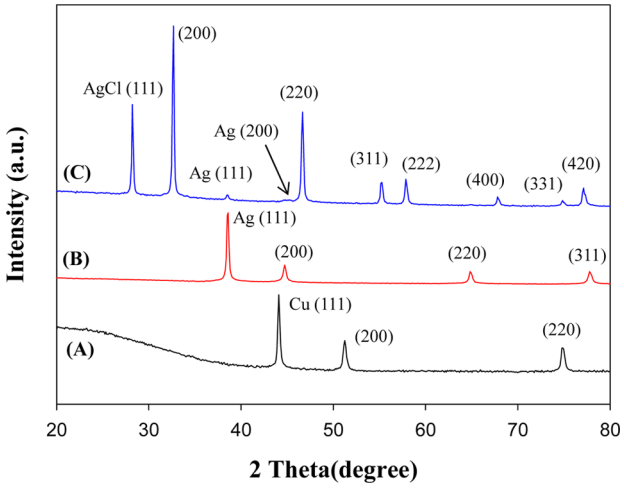


**Figure 3.** XRD spectra of the Cu nanowires (A), Ag nanotubes (B), and Ag@AgCl nanotubes (C).

(220), (311), (222), (400), (331), and (420) planes of the typical cubic phase of AgCl (JCPDS 31-1238). In Figure 3, spectrum C, the additional peaks at 38.6 and 44.7° from Ag (111) and Ag (200) can also be observed, although they are much weaker than those from AgCl. The XRD result indicates the coexistence of AgCl and Ag in the Ag@AgCl nanotubes. However, the weak diffraction peaks from Ag suggest the low content of metallic Ag in the Ag@AgCl composites.

The elemental composition and the chemical status of the produced Ag@AgCl nanotubes were analyzed by XPS measurements. The XPS survey spectrum of Ag@AgCl is shown in Figure 4A. The XPS signals from elements of Ag, Cl,

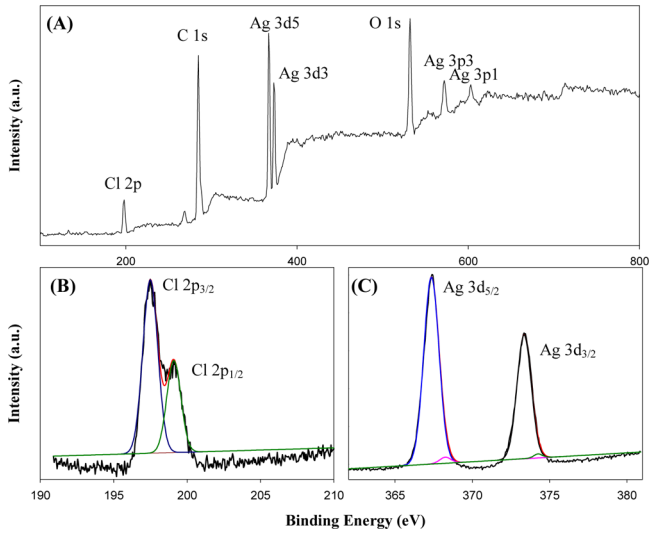


**Figure 4.** XPS survey spectrum (A) and XPS spectra of Cl 2p (B) and Ag 3d (C) of the as-prepared Ag@AgCl nanotubes.

C, and O can be seen. The Cl 2p XPS spectrum in Figure 4B displays double peaks at 197.5 and 199.1 eV, which could be assigned to the binding energies of Cl $2p_{3/2}$ and Cl $2p_{1/2}$, respectively.[26] The XPS spectrum of Ag 3d shown in Figure 4C could be deconvoluted into two doublets. The two peaks at 367.35 and 373.35 eV could be assigned to Ag $3d_{3/2}$ and Ag $3d_{5/2}$ of AgCl. Meanwhile, the other two peaks centered at 368.25 and 374.25 eV correspond to the metallic Ag.[9,23,27] The XPS result further confirms the low content of $Ag^0$ in the sample of Ag@AgCl nanotubes, consistent with the XRD result.

Light absorption properties of photocatalysts are very important for their application in degradation of organic dyes. Here, the light absorption of Ag nanotubes and Ag@AgCl nanotubes was also measured. From the UV−vis absorption spectra displayed in Figure 5, the Ag nanotubes show a wide, but no obvious peak, absorption from surface plasmon resonance. Such a phenomenon has also been observed in the UV−vis absorption spectrum of large Ag spheres.[27] Here, the large dimension of the as-prepared Ag nanotubes may result in the weak surface plasmon resonance. Compared to the silver nanotubes, the Ag@AgCl nanotubes exhibit enhanced absorption in both UV and visible light regions. The characteristic absorption of AgCl could account for the absorption within 200−350 nm. Meanwhile, the broad absorption in the range of 350−800 nm is probably from the surface plasmon absorption of Ag nanoparticles formed on the surface of Ag@AgCl nanotubes.[6,28] The strong absorption in the visible light region suggests that the Ag@AgCl nanotubes can efficiently utilize the sunlight for the degradation of organic pollutants.

**3.2. Photocatalytic Degradation of Methyl Orange (MO) over Ag@AgCl Nanotubes.** To compare the photocatalytic performances of the as-synthesized Ag@AgCl nano-

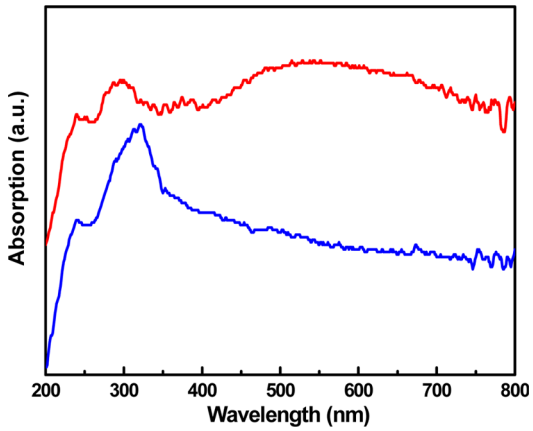


**Figure 5.** UV−vis diffuse reflectance spectra of the Ag nanotubes (blue curve) and Ag@AgCl nanotubes (1:1) (red curve).

tube samples (the molar ratios of Ag:Fe = 4:1, 2:1, 4:3, 1:1, and 2:3), the photodecomposition of MO was studied in aqueous dispersions under visible light irradiation. For comparison, the photodegradation of MO without catalyst (blank) and on Ag nanotubes and commercial $TiO_2$ catalyst (P25) was also investigated. Figure 6A shows the evolution of the absorption of MO with light irradiation time on the Ag@AgCl (1:1) nanotubes. It can be seen that MO was degraded efficiently by

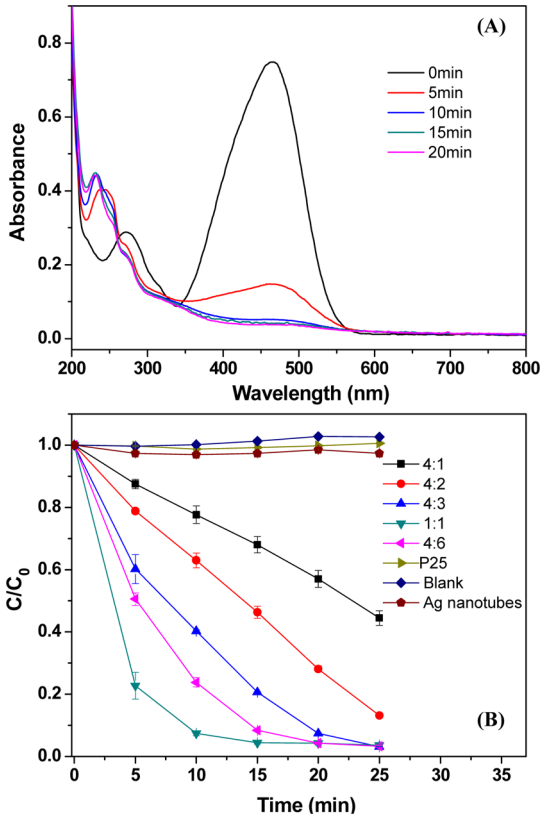


**Figure 6.** (A) UV−vis absorbance change of methyl orange (MO) as a function of visible light ($\lambda \geq 400$ nm) irradiation time on the as-prepared Ag@AgCl (1:1) nanotubes. (B) Photocatalytic activities for the degradation of MO dye under visible light irradiation without the presence of catalyst and over Ag nanotubes, commercial P25, and various Ag@AgCl samples with different molar ratios of Ag:Fe (4:1, 4:2, 4:3, 1:1, and 4:6).

the Ag@AgCl nanotubes under visible light, and after 10 min of irradiation, almost all MO has been decomposed. Figure 6B shows the visible light irradiation time-dependent degradation of MO on the studied photocatalysts, where $C_0$ represents the concentration of MO after the sufficient adsorption on the surface of catalysts and $C$ denotes the MO concentration after visible light irradiation for a certain time. Without the presence of photocatalyst (blank), negligible photodegradation of MO occurred. Over the silver nanotubes, only limited MO can be degraded under visible light. However, all the Ag@AgCl nanotube samples exhibited high photocatalytic performance for the degradation of an MO molecule. Moreover, the photocatalytic activities of the Ag@AgCl nanotubes strongly depend on the amount of added $FeCl_3$ (i.e., the ratio of Ag to Fe). In this system, the photocatalytic activity of the Ag@AgCl nanotubes first increases with increasing the ratio of Fe to Ag, and the sample with a 1:1 ratio exhibited the highest activity for the photodecomposition of MO dye. However, with the ratio of Fe/Ag further increasing, the photocatalytic activity will decrease. For instance, under the visible light irradiation for 10 min, 22.3, 37.0, 59.8, 92.6, and 76.2% of MO can be decomposed over the Ag@AgCl nanotubes with the Ag/Fe ratios of 4:1, 4:2, 4:3, 1:1, and 4:6, respectively. On the basis of the previous reports,[13,29] different molar ratios of Ag and $FeCl_3$ may lead to the changes of the product in composition, microstructure, and morphology. Such complicated effects and the growth mechanism of the hollow tubulate structure need to be further investigated. It should be noted that the commercial P25 photocatalyst has almost no photocatalytic activity for MO decomposition under visible light. The previous studies showed that P25 is a kind of good photocatalyst for the decomposition of dye pollutants under the condition of UV−vis irradiation. Suppose that the photodecomposition of MO has a pseudo-first-order reaction mechanism, the decomposition rates of MO on the Ag@AgCl nanotube catalysts with the different Ag:Fe molar ratios of 4:1, 4:2, 4:3, 1:1, and 4:6 were estimated to be 0.0313, 0.0774, 0.1386, 0.2601, and 0.1459 $min^{-1}$, respectively. Meanwhile, we also studied the photodegradation of Rhodamine B (RhB) dye over the Ag@AgCl nanotubes, and the results (Figure S1, Supporting Information) showed the similar trends to that of the MO degradation. These experimental results clearly demonstrate that the synthesized hollow Ag@AgCl samples could serve as a type of photocatalyst for the efficient degradation of dye pollutants.

In order to exclude the dyes' self-photosensitized effect, phenol, a typical colorless pollutant with no absorption in the visible region, was also chosen as a reference molecule to further evaluate the photocatalytic activity of the synthesized hollow tubulate Ag@AgCl (Ag:Fe = 1:1) nanostructures under visible light. As shown in Figure S2A (Supporting Information), the evolution of the absorbance of phenol with irradiation time on the Ag@AgCl (1:1) nanotubes can be clearly identified. From Figure S2B, one can see that, under irradiation of visible light for 180 min, negligible photodegradation of phenol occurred in the direct photolysis without the Ag@AgCl catalyst (red curve), whereas nearly 88% of phenol has been degraded with the presence of Ag@AgCl (1:1) nanotubes. Such results strongly indicate that the Ag@AgCl hollow nanotubes in the present study could be a class of promising visible light photocatalysts.

The morphology effects of Ag@AgCl hybrids on their photocatalytic activities were also investigated. Ag nanowires were synthesized according to the previously reported

procedure.[30] Ag@AgCl composites were then synthesized using the above method through the in situ oxidation of the silver nanowires by $FeCl_3$ (the ratio of Ag:Fe = 1:1) in aqueous poly(vinylpyrrolidone) solution at room temperature. Figure S3A (Supporting Information) shows the representative TEM image of the as-produced Ag nanowires, which indicates that uniform Ag nanowires with an average diameter of 110 nm have been synthesized. From the TEM image shown in Figure S3B, Ag@AgCl heterostructured porous nanowires have been produced with an increased diameter of about 500 nm by using silver nanowires as templates. The photocatalytic activities of the Ag@AgCl hollow nanotubes and the almost same-sized Ag@AgCl porous nanowires for the degradation of MO dyes were compared. As shown in Figure S3C, under visible light irradiation for 10 min, 92.58% and 79.94% of MO can be decomposed over the Ag@AgCl (the Ag/Fe ratio of 1:1) nanotubes and the porous nanowires, respectively, indicating the morphology effect of Ag@AgCl on their photocatalytic performance. On the basis of the above results, the tubulate morphology is beneficial to the visible light photocatalysis.

The photostability is important for the real application of a photocatalyst. In order to study the structural and catalytic stability of the Ag@AgCl nanotubes, the photocatalytic degradation of MO was repeated four times, and the morphology and crystal structure of the material were then examined. As shown in Figure 7, after four-cycle tests of MO photodecomposition, there is no obvious loss of photocatalytic activity of the catalyst, indicating the excellent photocatalytic stability of the Ag@AgCl nanotubes. The XRD pattern and SEM image of the sample after the repeated photocatalytic experiments were measured and are shown in Figure 8. One can see that the XRD pattern still shows the sharp and strong diffraction peaks from the cubic phase of AgCl, almost identical to that of the as-prepared sample. The SEM image shows that the sample still maintains the tubulate morphology. These results strongly indicate that the Ag@AgCl nanotubes are very stable as photocatalysts under visible light irradiation.

To fully understand the photocatalytic property of the Ag@AgCl nanotubes, the possible mechanism of photocatalytic degradation of MO on the hybrid was proposed. As shown in Figure 9, for the Ag@AgCl nanotubes, photogenerated

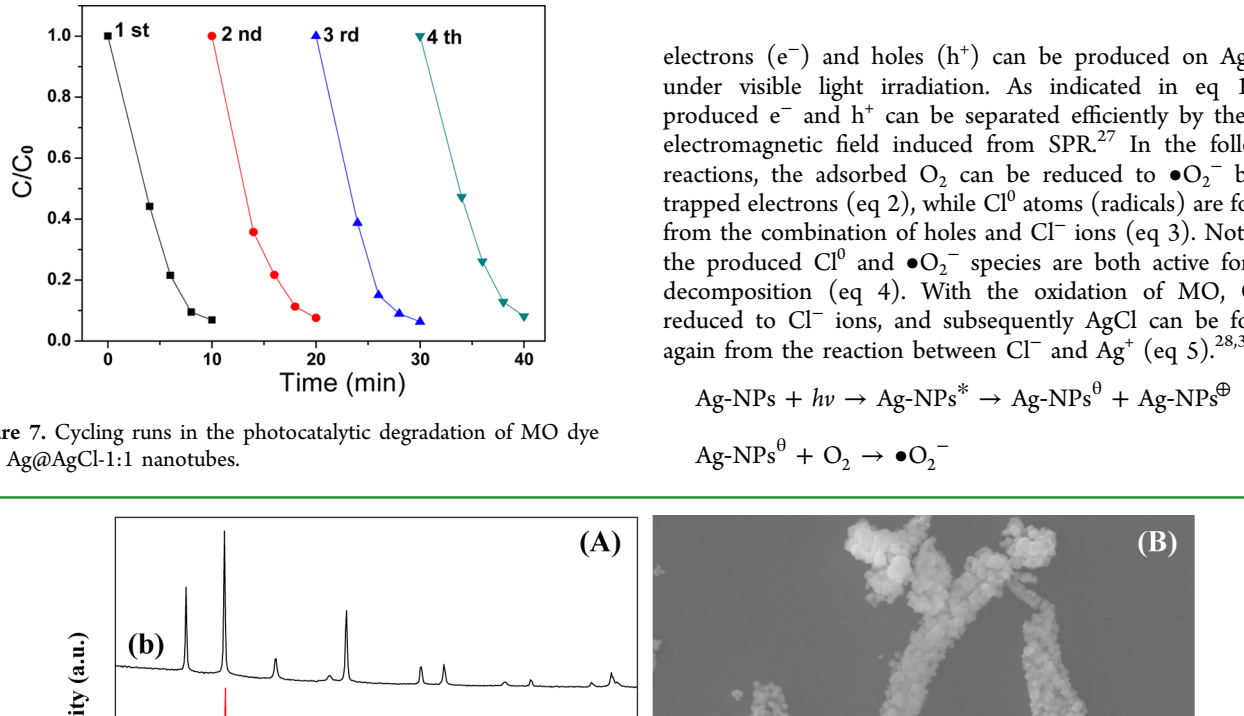


**Figure 7.** Cycling runs in the photocatalytic degradation of MO dye over Ag@AgCl-1:1 nanotubes.

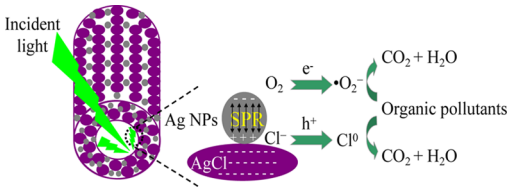


**Figure 9.** Schematic illustration of the photocatalytic degradation mechanism of organic dyes over the Ag@AgCl nanotubes under visible light irradiation.

electrons ($e^-$) and holes ($h^+$) can be produced on Ag NPs under visible light irradiation. As indicated in eq 1, the produced $e^-$ and $h^+$ can be separated efficiently by the local electromagnetic field induced from SPR.[27] In the following reactions, the adsorbed $O_2$ can be reduced to $\bullet O_2^-$ by the trapped electrons (eq 2), while $Cl^0$ atoms (radicals) are formed from the combination of holes and $Cl^-$ ions (eq 3). Note that the produced $Cl^0$ and $\bullet O_2^-$ species are both active for MO decomposition (eq 4). With the oxidation of MO, $Cl^0$ is reduced to $Cl^-$ ions, and subsequently AgCl can be formed again from the reaction between $Cl^-$ and $Ag^+$ (eq 5).[28,31−33]

$$\text{Ag-NPs} + h\nu \rightarrow \text{Ag-NPs}^* \rightarrow \text{Ag-NPs}^{\theta} + \text{Ag-NPs}^{\oplus} \quad (1)$$

$$\text{Ag-NPs}^{\theta} + O_2 \rightarrow \bullet O_2^- \quad (2)$$

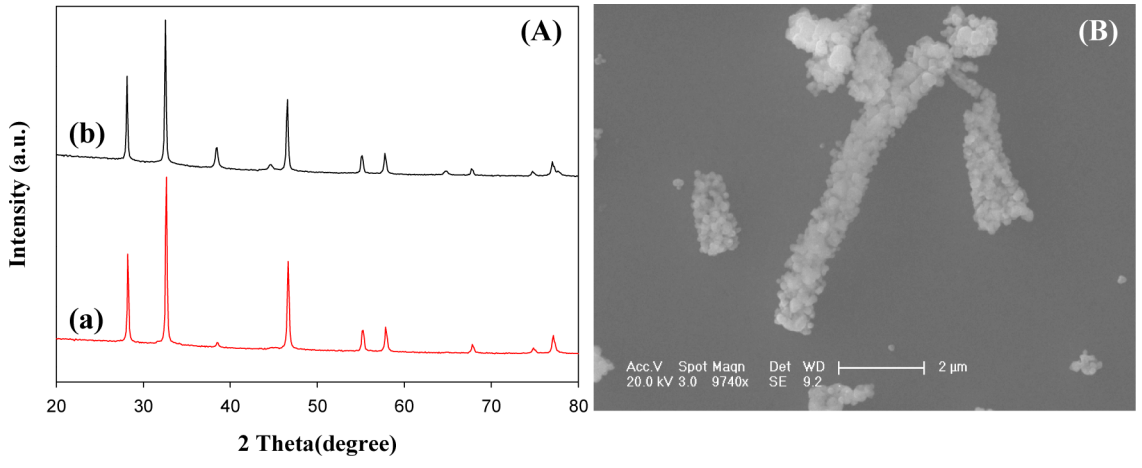


**Figure 8.** (A) XRD spectra of the Ag@AgCl nanotubes before (a) and after (b) the photocatalytic degradation of the MO. (B) SEM image of the Ag@AgCl nanotubes after the experiment of MO degradation.

$$\text{Ag-NPs}^{\oplus} + \text{AgCl} \rightarrow \text{Cl}^0 + \text{Ag}^+ \quad (3)$$

$$\text{Cl}^0 + \text{MO} \rightarrow \text{degraded products} + \text{Cl}^- \text{ or}$$
$$\bullet\text{O}_2^- (\bullet\text{OH}) + \text{MO} \rightarrow \text{degraded products} \quad (4)$$

$$\text{Ag}^+ + \text{Cl}^- \rightarrow \text{AgCl} \quad (5)$$

## 4. CONCLUSIONS

In summary, the plasmonic photocatalyst Ag@AgCl nanotubes were successfully synthesized through a simple galvanic replacement reaction with copper nanowires as a template, followed by the in situ oxidation by $FeCl_3$. TEM, XRD, EDX, and XPS measurements showed that, with the present synthetic strategy, tubulate product can be produced and the original copper wire can be completely converted to Ag@AgCl nanotubes. The as-synthesized hybrid nanotubes showed high photocatalytic activity for the decomposition of methyl orange under visible light irradiation. The photocatalytic activity of the Ag@AgCl nanotubes was found to depend on the added $FeCl_3$. The sample with a 1:1 ratio of Fe/Ag exhibited the highest photocatalytic performance, and more than 92.58% of MO dye was degraded within 10 min. In addition, the photocatalytic activity and structure of the Ag@AgCl nanotubes exhibited high stability, with almost no activity loss after at least four cycles of photocatalytic reaction. The enhanced photocatalytic performance of the Ag@AgCl composites can be mainly attributed to their unique tubulate and porous structure with enhanced surface area for dye adsorption and strong visible light absorbance, and the hybrid structure for efficient charge separation. With the efficient visible light absorption and high photocatalytic activity and stability, the Ag@AgCl nanotube photocatalysts have promising application in photocatalysis for degradation of organic pollutants and purification of water.

## ■ ASSOCIATED CONTENT

### Supporting Information

Photocatalytic activities of Ag@AgCl nanotubes for the degradation of Rhodamine B and phenol under visible light irradiation, TEM image, and photocatalytic property of Ag@AgCl porous nanowires for the degradation of MO under visible light irradiation. This material is available free of charge via the Internet at http://pubs.acs.org.

## ■ AUTHOR INFORMATION

### Corresponding Author

*E-mail: weichen@ciac.ac.cn (W.C.).

### Author Contributions

[‖]These authors contributed equally to this work.

### Notes

The authors declare no competing financial interest.

## ■ ACKNOWLEDGMENTS

This work was supported by the National Natural Science Foundation of China (No. 21275136) and the Natural Science Foundation of Jilin province, China (No. 201215090).

## ■ REFERENCES

(1) Aksu, Z. Application of Biosorption for the Removal of Organic Pollutants: A Review. *Process Biochem.* **2005**, *40*, 997−1026.

(2) Hoffmann, M. R.; Martin, S. T.; Choi, W. Y.; Bahnemann, D. W. Environmental Applications of Semiconductor Photocatalysis. *Chem. Rev.* **1995**, *95*, 69−96.

(3) Zhang, J. L.; Wu, Y. M.; Xing, M. Y.; Leghari, S. A. K.; Sajjad, S. Development of Modified N Doped $TiO_2$ Photocatalyst with Metals, Nonmetals and Metal Oxides. *Energy Environ. Sci.* **2010**, *3*, 715−726.

(4) Wang, P.; Huang, B. B.; Dai, Y.; Whangbo, M. H. Plasmonic Photocatalysts: Harvesting Visible Light with Noble Metal Nanoparticles. *Phys. Chem. Chem. Phys.* **2012**, *14*, 9813−9825.

(5) Xu, Y. G.; Xu, H.; Yan, J.; Li, H. M.; Huang, L. Y.; Zhang, Q.; Huang, C. J.; Wan, H. L. A Novel Visible-Light-Response Plasmonic Photocatalyst CNT/Ag/AgBr and Its Photocatalytic Properties. *Phys. Chem. Chem. Phys.* **2013**, *15*, 5821−5830.

(6) Han, L.; Wang, P.; Zhu, C. Z.; Zhai, Y. M.; Dong, S. J. Facile Solvothermal Synthesis of Cube-like Ag@AgCl: A Highly Efficient Visible Light Photocatalyst. *Nanoscale* **2011**, *3*, 2931−2935.

(7) Kuai, L.; Geng, B. Y.; Chen, X. T.; Zhao, Y. Y.; Luo, Y. C. Facile Subsequently Light-Induced Route to Highly Efficient and Stable Sunlight-Driven Ag-AgBr Plasmonic Photocatalyst. *Langmuir* **2010**, *26*, 18723−18727.

(8) Wang, P.; Huang, B. B.; Zhang, Q. Q.; Zhang, X. Y.; Qin, X. Y.; Dai, Y.; Zhan, J.; Yu, J. X.; Liu, H. X.; Lou, Z. Z. Highly Efficient Visible Light Plasmonic Photocatalyst Ag@Ag(Br,I). *Chem.—Eur. J.* **2010**, *16*, 10042−10047.

(9) Ai, L. H.; Zhang, C. H.; Jiang, J. Hierarchical Porous AgCl@Ag Hollow Architectures: Self-Templating Synthesis and Highly Enhanced Visible Light Photocatalytic Activity. *Appl. Catal., B* **2013**, *142*, 744−751.

(10) Li, Y. Y.; Ding, Y. Porous AgCl/Ag Nanocomposites with Enhanced Visible Light Photocatalytic Properties. *J. Phys. Chem. C* **2010**, *114*, 3175−3179.

(11) An, C. H.; Wang, R. P.; Wang, S. T.; Zhang, X. Y. Converting AgCl Nanocubes to Sunlight-Driven Plasmonic AgCl:Ag Nanophotocatalyst with High Activity and Durability. *J. Mater. Chem.* **2011**, *21*, 11532−11536.

(12) Lou, Z. Z.; Huang, B. B.; Wang, P.; Wang, Z. Y.; Qin, X. Y.; Zhang, X. Y.; Cheng, H. F.; Zheng, Z. K.; Dai, Y. The Synthesis of the Near-Spherical AgCl Crystal for Visible Light Photocatalytic Applications. *Dalton Trans.* **2011**, *40*, 4104−4110.

(13) Jia, C. C.; Yang, P.; Huang, B. B. Uniform Ag/AgCl Necklace-like Nano-Heterostructures: Fabrication and Highly Efficient Plasmonic Photocatalysis. *ChemCatChem* **2014**, *6*, 611−617.

(14) Wang, Z. X.; Chen, M.; Wu, L. M. Synthesis of Monodisperse Hollow Silver Spheres Using Phase-Transformable Emulsions as Templates. *Chem. Mater.* **2008**, *20*, 3251−3253.

(15) Lou, X. W.; Archer, L. A.; Yang, Z. C. Hollow Micro-/Nanostructures: Synthesis and Applications. *Adv. Mater.* **2008**, *20*, 3987−4019.

(16) Sun, Y. G.; Mayers, B.; Xia, Y. N. Metal Nanostructures with Hollow Interiors. *Adv. Mater.* **2003**, *15*, 641−646.

(17) Ai, L. H.; Jiang, J. Hierarchical Porous Quaternary Cu-Fe-Sn-S Hollow Chain Microspheres: Rapid Microwave Nonaqueous Synthesis, Growth Mechanism, and Their Efficient Removal of Organic Dye Pollutant in Water. *J. Mater. Chem.* **2012**, *22*, 20586−20592.

(18) Cheng, H. F.; Huang, B. B.; Liu, Y. Y.; Wang, Z. Y.; Qin, X. Y.; Zhang, X. Y.; Dai, Y. An Anion Exchange Approach to $Bi_2WO_6$ Hollow Microspheres with Efficient Visible Light Photocatalytic Reduction of CO2 to Methanol. *Chem. Commun.* **2012**, *48*, 9729−9731.

(19) Li, X. N.; Huang, R. K.; Hu, Y. H.; Chen, Y. J.; Liu, W. J.; Yuan, R. S.; Li, Z. H. A Ternplated Method to $Bi_2WO_6$ Hollow Microspheres and Their Conversion to Double-Shell $Bi_2O_3/Bi_2WO_6$ Hollow Microspheres with Improved Photocatalytic Performance. *Inorg. Chem.* **2012**, *51*, 6245−6250.

(20) Yu, X. X.; Yu, J. G.; Cheng, B.; Huang, B. B. One-Pot Template-Free Synthesis of Monodisperse Zinc Sulfide Hollow Spheres and Their Photocatalytic Properties. *Chem.—Eur. J.* **2009**, *15*, 6731−6739.

(21) Tu, W. G.; Zhou, Y.; Liu, Q.; Tian, Z. P.; Gao, J.; Chen, X. Y.; Zhang, H. T.; Liu, J. G.; Zou, Z. G. Robust Hollow Spheres Consisting of Alternating Titania Nanosheets and Graphene Nanosheets with

High Photocatalytic Activity for $CO_2$ Conversion into Renewable Fuels. *Adv. Funct. Mater.* **2012**, *22*, 1215−1221.
(22) Tang, Y. X.; Jiang, Z. L.; Xing, G. C.; Li, A. R.; Kanhere, P. D.; Zhang, Y. Y.; Sum, T. C.; Li, S. Z.; Chen, X. D.; Dong, Z. L.; Chen, Z. Efficient Ag@AgCl Cubic Cage Photocatalysts Profit from Ultrafast Plasmon-Induced Electron Transfer Processes. *Adv. Funct. Mater.* **2013**, *23*, 2932−2940.
(23) Wang, P.; Huang, B. B.; Lou, Z. Z.; Zhang, X. Y.; Qin, X. Y.; Dai, Y.; Zheng, Z. K.; Wang, X. N. Synthesis of Highly Efficient Ag@AgCl Plasmonic Photocatalysts with Various Structures. *Chem.—Eur. J.* **2010**, *16*, 538−544.
(24) Lu, X. F.; McKiernan, M.; Peng, Z. M.; Lee, E. P.; Yang, H.; Xia, Y. N. Noble-Metal Nanotubes Prepared via a Galvanic Replacement Reaction Between Cu Nanowires and Aqueous $HAuCl_4$, $H_2PtCl_6$, or $Na_2PdCl_4$. *Sci. Adv. Mater.* **2010**, *2*, 413−420.
(25) Rathmell, A. R.; Bergin, S. M.; Hua, Y. L.; Li, Z. Y.; Wiley, B. J. The Growth Mechanism of Copper Nanowires and Their Properties in Flexible, Transparent Conducting Films. *Adv. Mater.* **2010**, *22*, 3558−3563.
(26) Dong, L. H.; Liang, D. D.; Gong, R. C. In Situ Photoactivated AgCl/Ag Nanocomposites with Enhanced Visible Light Photocatalytic and Antibacterial Activity. *Eur. J. Inorg. Chem.* **2012**, 3200−3208.
(27) Dong, R. F.; Tian, B. Z.; Zeng, C. Y.; Li, T. Y.; Wang, T. T.; Zhang, J. L. Ecofriendly Synthesis and Photocatalytic Activity of Uniform Cubic Ag@AgCl Plasmonic Photocatalyst. *J. Phys. Chem. C* **2013**, *117*, 213−220.
(28) Ma, B. W.; Guo, J. F.; Dai, W. L.; Fan, K. N. Highly Stable and Efficient Ag/AgCl Core-Shell Sphere: Controllable Synthesis, Characterization, and Photocatalytic Application. *Appl. Catal., B* **2013**, *130*, 257−263.
(29) Bi, Y. P.; Ye, J. H. In situ Oxidation Synthesis of Ag/AgCl Core-Shell Nanowires and Their Photocatalytic Properties. *Chem. Commun.* **2009**, 6551−6553.
(30) Lu, Y.; Chen, W. Nanoneedle-Covered Pd−Ag Nanotubes: High Electrocatalytic Activity for Formic Acid Oxidation. *J. Phys. Chem. C* **2010**, *114*, 21190−21200.
(31) Xu, Y. G.; Xu, H.; Li, H. M.; Yan, J.; Xia, J. X.; Yin, S.; Zhang, Q. Ionic Liquid Oxidation Synthesis of Ag@AgCl Core-Shell Structure for Photocatalytic Application under Visible-Light Orradiation. *Colloids Surf., A* **2013**, *416*, 80−85.
(32) Xu, H.; Li, H. M.; Xia, J. X.; Yin, S.; Luo, Z. J.; Liu, L.; Xu, L. One-Pot Synthesis of Visible-Light-Driven Plasmonic Photocatalyst Ag/AgCl in Ionic Liquid. *ACS Appl. Mater. Interfaces* **2011**, *3*, 22−29.
(33) Wang, P.; Huang, B.; Qin, X.; Zhang, X.; Dai, Y.; Wei, J.; Whangbo, M.-H. Ag@AgCl: A Highly Efficient and Stable Photocatalyst Active under Visible Light. *Angew. Chem., Int. Ed.* **2008**, *47*, 7931−7933.